

Chapter 13 Thermodynamic Feedbacks in the Climate System

The Earth's climate varies over many time scales, ranging from interannual and interdecadal variations to changes on geological time scales associated with ice ages and continental drift. The climate can vary either because of alterations in the internal dynamics and exchanges of energy within the climate system, or from external forcing. Examples of external climate forcing include variations in the amount and latitudinal distribution of solar radiation at the top of the atmosphere, varying amounts of greenhouse gases (*e.g.*, CO₂) caused by human activity, and variations in volcanic activity.

To understand and simulate climate and climate change, it is necessary to interpret the role of various physical processes in determining the magnitude of the climate response to a specific forcing. The large number of interrelated physical processes acting at different rates within and between the components of the climate system makes this interpretation a difficult task. An anomaly in one part of the system may set off a series of adjustments throughout the rest of the climate system, depending on the nature, location, and size of the initial disturbance.

The relationship between the magnitude of the climate forcing and the magnitude of the climate change response defines the *climate sensitivity*. A process that changes the sensitivity of the climate response is called a *feedback mechanism*. A feedback is positive if the process increases the magnitude of the response and negative if the feedback reduces the magnitude of the response. The concepts behind feedbacks as applied to climate change are derived from concepts in control theory that were first developed for electronics. By examining separate feedback loops, one can gain a sense of the direction of the influence of the feedback on a change in the state of the system, whether it is reinforcing or damping, and the relative importance of a given feedback when compared with other feedbacks. Climate change can therefore be viewed as the result of adjustment among compensating feedback processes, each of which behaves in a characteristically nonlinear fashion. The fact that the climate of the Earth has varied in the past between rather narrow limits despite large variations in external forcing is evidence for the efficiency and robustness of these feedbacks.

A variety of climate feedback mechanisms have been identified, including radiation feedbacks that involve water vapor and clouds, ocean feedbacks that involve the hydrological cycle, and biospheric feedbacks that involve the carbon cycle. In our consideration of thermodynamic feedbacks in the climate system, we will concentrate on the radiative and

ocean thermohaline feedbacks. The radiation feedback processes that are of interest in the context of the climate system include the snow/ice-albedo feedback, water vapor feedback, and cloud-radiation feedbacks.

13.1 Introduction to Feedback and Control Systems

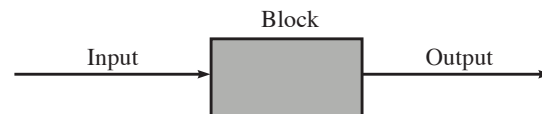
A *control system* is an arrangement of physical components that are connected in such a manner as to regulate itself or another system. The *input* to a control system is the stimulus from an external energy source that produces a specified response from the control system. The *output* is the actual response obtained from the control system.

An *open-loop* control system is one in which the control action is independent of the output. A *closed-loop* control system is one in which the control action is somehow dependent on the output. Closed-loop control systems are more commonly called *feedback control systems*. Feedback is said to exist in a system when a closed sequence of cause-and-effect relations exists between system variables.

In order to solve a control systems problem, the specifications or description of the system configuration and its components must be put into a form amenable to analysis and evaluation. Three basic representations (models) are employed in the study of control systems:

1. block diagrams
2. signal flow graphs
3. differential equations and other mathematical relations

A *block diagram* is a shorthand, graphical representation of cause and effect relationships between the input and output of a control system. It provides a convenient and useful method for characterizing the functional relationships among the various components of a control system. System components are also called *elements* of the system. The simplest form of the block diagram is the single block, with one input and one output:



The *input* is the stimulus applied to a control system from an external energy source. The *output* is the actual response obtained from a control system, which may or may not be equal to the specified response implied by the input. The basic configuration of a simple closed-loop (feedback) control system is illustrated in Figure 13.1. In the absence of feedback, the term G_o represents the *gain* of the system, which is the ratio of output to input. The *feedback* F is the component required to establish the functional relationship between the primary feedback signal and the

controlled output. It is emphasized that the arrows of the closed loop, connecting one block with another, represent the flow of control energy or information, and not the main source of energy for the system.

A *signal flow graph* displays pictorially the transmission of signals through the system, as does the block diagram; however a signal flow graph is easier to construct than the block diagram. A signal flow graph is shown in Figure 13.2, corresponding to the block diagram shown in Figure 13.1. A *feedback loop* is a path which originates and terminates on the same node. For example, in Figure 13.2, *C* to *E* and back to *C* is a feedback loop.

Referring to Figures 13.1 and 13.2, we define the following parameters. The *feedback factor*, f , is defined as:

$$f = G_o F \quad (13.1a)$$

The *gain of the system in the presence of feedbacks* is given by G_f , which is also referred to as the *control ratio*:

$$G_f = \frac{G_o}{1-f} \quad (13.1b)$$

We define the *feedback gain ratio* as

$$\mathcal{R}_f = \frac{G_f}{G_o} = \frac{1}{1-f} \quad (13.1c)$$

Mathematical models, in the form of system equations, are employed when detailed relationships are required. Every control system may be characterized theoretically by mathematical equations. Often, however, a solution is difficult if not impossible to find. In these cases, certain simplifying assumptions must be made in the mathematical description, typically leading to systems that can be described by linear ordinary differential equations.

Evaluations of feedbacks in the climate system are useful in the following contexts:

- conceptual understanding of how the climate system operates
- evaluation of climate model performance
- quantification of climate system response to different forcing and the role played by various physical processes

Applications of the theory of feedback control systems to the Earth's climate are considered in the following sections.

13.2 Radiation Climate Sensitivity and Feedbacks

We may express a climate system in the following manner

$$L = L(X) = L(X_1, X_2, \dots)$$

where

$$X_1 = X_1(L, X) = X_1(X_2, X_3, \dots)$$

In this nonlinear system, L describes a family of climate variables which depend on X_i . In a fully interactive (closed-loop) system, X_1 may also be a function of L and X_i . In an open-loop system, X_1 is a constant and therefore changes to the climate system, which are produced by a change in specification of X_1 , are not allowed to feedback onto X_1 . The *sensitivity*, δ , of the climate variable X_2 to a change in X_1 is defined as

$$\delta = \frac{X_1}{X_2} \frac{\partial X_2}{\partial X_1} \quad (13.2)$$

An example of a tractable closed-loop climate system is a simple planetary energy balance model (as described in Section 12.1) that is used to examine radiative feedback processes in the Earth's climate (following Schlesinger, 1986). A planetary energy balance climate model predicts the change in temperature at the Earth's surface, ΔT_0 , from the requirement that $\Delta F_{TOA}^{rad} = 0$, where F_{TOA}^{rad} is the net radiative flux at the top of the atmosphere from (12.1b)

$$F_{TOA}^{rad} = \frac{\Sigma}{4} (1 - \alpha_p) - F_{TOA}^{LW}$$

F_{TOA}^{LW} is the upwelling longwave radiation at the top of the atmosphere, frequently referred to as *outgoing longwave radiation* (OLR), and α_p is the planetary albedo. To assess changes in the net radiative flux at the top of the atmosphere, F_{TOA}^{rad} can be expressed as a symbolic function L

$$F_{TOA}^{rad} = L(E_i, T_0, I_j) \quad (13.3)$$

The term E_i represents quantities that can be regarded as external to the climate system, which are quantities whose change can lead to change in climate but are independent of the climate (*e.g.*, volcanic eruptions, change in solar output). The term I_j represents quantities that are internal to the climate system, which are quantities that can change as the climate changes, and in so doing feedback to modify the climate change. The internal quantities include all of the variables of the climate system other than T_0 . Because T_0 is the only dependent variable in the energy

balance climate model, the internal quantities must be represented as a function of T_0 .

A small change in the energy flux at the top of the atmosphere ΔF_{TOA}^{rad} can be expressed in terms of E_i , T_0 , and I_j as

$$\Delta F_{TOA}^{rad} = \sum_i \frac{\partial F_{TOA}^{rad}}{\partial E_i} \Delta E_i + \left[\frac{\partial F_{TOA}^{rad}}{\partial T_0} + \sum_j \frac{\partial F_{TOA}^{rad}}{\partial I_j} \frac{dI_j}{dT_0} \right] \Delta T_0 \quad (13.4)$$

By examining Figure 13.1 and (13.4), we can identify the following relationships:

$$\text{input: } \frac{\partial F_{TOA}^{rad}}{\partial E_i} \Delta E_i \equiv \Delta Q \quad (13.5)$$

$$\text{output: } \Delta T_0$$

$$\mathcal{G}_o^{-1} = \frac{\partial F_{TOA}^{rad}}{\partial T_0} \quad (13.6)$$

$$\mathcal{F} = \sum_j \frac{\partial F_{TOA}^{rad}}{\partial I_j} \frac{dI_j}{dT_0} \quad (13.7)$$

$$f = \mathcal{G}_o \sum_j \frac{\partial F_{TOA}^{rad}}{\partial I_j} \frac{dI_j}{dT_0} \quad (13.8)$$

where we have defined a new variable Q in (13.5), which is referred to as the *external climate input*.

Incorporating the above relationships into (13.5), we obtain

$$\Delta F_{TOA}^{rad} = \Delta Q + (\mathcal{G}_o^{-1} - \mathcal{F}) \Delta T_0 = \Delta Q - \mathcal{G}_f^{-1} \Delta T_0 \quad (13.9)$$

Using the energy balance requirement that $\Delta F_{TOA}^{rad} = 0$, we obtain

$$\Delta T_0 = \mathcal{G}_f \Delta Q \quad (13.10a)$$

If $\mathcal{F} \neq 0$, the response of the surface temperature, ΔT_0 , to the forcing, ΔQ , is modulated by feedback. If $\mathcal{F} = 0$, we have

$$\Delta T_0 = (\Delta T_0)^* = \mathcal{G}_o \Delta Q \quad (13.10b)$$

where $(\Delta T_0)^*$ represents the zero-feedback temperature change.

From the definition of the feedback gain ratio, we can write

$$\mathcal{R}_f = \frac{G_f}{G_o} = \frac{1}{1-f} = \frac{\Delta T_0}{(\Delta T_0)^*} \quad (13.11)$$

Figure 13.3 plots the feedback gain ratio, \mathcal{R}_f , against the feedback, f . Values of $f < 0$ and $0 < \mathcal{R}_f < 1$ represents negative feedback. Values of $\mathcal{R}_f > 1$ for $0 < f < 1$ represents positive feedback.

This simple application of control theory has considered a linear climate system. The expression for the feedback parameter

$$f = G_o \sum_j \frac{\partial F_{TOA}^{rad}}{\partial I_j} \frac{dI_j}{dT_0}$$

derived from this analysis assumes that the feedbacks are additive and thus independent. In principle, the contribution of each mechanism to the total feedback could be individually determined and ranked. In a nonlinear system, however, the feedbacks are not independent and addition of the individual terms will not give the true feedback of the nonlinear climate system. Applications of this type of linear feedback analysis have been made to the climate system, justified by considering only small perturbations to the radiative flux and surface temperature. Because of the difficulty of nonlinear control analysis, particularly for a system as complex as the climate system, no attempt has been made to apply control theory to the climate system beyond the type of linear analysis described above.

In spite of its simplicity, the linear analysis described here can be used to provide useful insights about the climate system. Direct evaluation of the feedback gain ratio, \mathcal{R}_f , from (13.11) (and then f from (13.8)) using a numerical model can be done in the following way. Three different model simulations are required:

1. a baseline simulation, representing the current unperturbed climate conditions
2. a simulation in which the climate is subject to an external perturbation and all feedbacks are operative
3. a run in which the climate is subject to an external perturbation, and selected feedbacks are “turned off” (for example, the snow/ice albedo feedback mechanism can be switched off by keeping the surface albedo fixed in the perturbed run to the same values used in the baseline simulation).

The feedback gain ratio is then evaluated from

$$\mathcal{R}_f = \frac{\Delta T_0}{(\Delta T_0)^*} = \frac{(T_0)_2 - (T_0)_1}{(T_0)_3 - (T_0)_1} \quad (13.12)$$

where the numerical subscripts refer to the enumerated model simulations above. This method of determining the feedbacks has the advantage that the feedbacks are not assumed *ab initio* to be additive.

An alternative application of the linear analysis is the evaluation of sensitivity. Examination of the feedback factor

$$f = G_o \sum_j \frac{\partial F_{TOA}^{rad}}{\partial I_i} \frac{dI_i}{dT_0}$$

shows that the following term can be identified with the sensitivity, δ (13.2)

$$\delta = G_o \frac{\partial F_{TOA}^{rad}}{\partial I_i} \quad (13.13)$$

The sensitivity of the radiative flux to changes in climate variables such as water vapor amount and cloud characteristics can then be determined from (13.13).

The individual feedback terms and net feedback determined from expressions like (13.12) must be interpreted with due caution, because of the nonlinearity of the system and the associated feedbacks. However, the signs of the individual feedback terms determined from (13.12) will probably be correct in response to a small perturbation to the climate system. Additionally, the sensitivity terms themselves provide useful diagnostics of the climate system and numerical simulations. To simulate feedbacks correctly, it is necessary (but not sufficient) for a climate model to reproduce the observed derivatives.

The general approach here outlined for a planetary energy balance model can also be applied easily to determine feedbacks in other simple models such as a surface energy balance model or radiative-convective model.

13.3 Water Vapor Feedback

The feedback between surface temperature, water vapor, and the Earth's radiation balance is referred to as the *water vapor feedback*. The water vapor feedback may be written following (13.12) as

$$f = G_o \frac{\partial F^{rad}}{\partial \mathcal{W}_v} \frac{d\mathcal{W}_v}{dT_0} \quad (13.15)$$

where \mathcal{W}_v is the vertically-integrated amount of water vapor (precipitable water; (4.41)).

Since water vapor emits strongly in the thermal (infrared) part of the spectrum, the net radiative flux at both the top of the atmosphere and at

the surface increases as the amount of water vapor increases (positive $\partial F^{ad}/\partial \mathcal{W}_v$). The concentration of water vapor decreases approximately exponentially with height (see Figure 1.1) and is very small in the stratosphere. The outgoing longwave radiation flux (OLR) at the top of the atmosphere, F_{TOA}^{LW} , decreases with increasing water vapor amount, since water vapor in the atmosphere emits at a colder temperature than the surface. The downwelling longwave radiation flux at the surface increases with increasing water vapor amount.

Climate modeling results have shown that the water vapor path increases with increasing surface temperature ($d\mathcal{W}_v/dT_0 > 0$). This increase arises from increased evaporation from a warmer ocean surface, providing additional water vapor to the atmosphere. A consistent result of climate models has been that atmospheric relative humidity remains approximately constant in a perturbed climate and that the water vapor feedback is among the chief mechanisms amplifying the global climate response to a perturbation. Since condensation and precipitation are associated with important sources and sinks of water vapor (Section 8.6), the water vapor feedback simulated by climate models depends on the model's parameterizations of cloud, precipitation, and convective processes. Given the current deficiencies in climate model parameterization of these processes, the water vapor feedback determined by these models must be questioned.

A more thorough understanding of $d\mathcal{W}_v/dT_0$ and the water vapor feedback can be obtained by using (4.41) to expand the derivative $d\mathcal{W}_v/dT_0$ as¹

$$\frac{d\mathcal{W}_v}{dT_0} = \frac{d}{dT_0} \frac{1}{\bar{g}} \int_0^{p_0} w_v dp = \frac{1}{\bar{g}} \int_0^{p_0} \frac{dw_v}{dT_0} dp \quad (13.16)$$

Using the definition of the water vapor mixing ratio (4.36), the derivative dw_v/dT_0 can be written as

$$\frac{dw_v}{dT_0} = \frac{\varepsilon}{\bar{p}} \left[e_s(p) \frac{\partial \mathcal{H}(p)}{\partial T_0} + \mathcal{H}(p) \frac{\partial e_s(p)}{\partial T_0} \right] \quad (13.17)$$

¹ Let $\phi(\alpha) = \int_{u_1}^{u_2} f(x, \alpha) dx$

where u_1 and u_2 may depend on the parameter α . Then

$$\frac{d\phi}{d\alpha} = \int_{u_1}^{u_2} \frac{\partial f}{\partial \alpha} dx + f(u_2, \alpha) \frac{du_2}{d\alpha} - f(u_1, \alpha) \frac{du_1}{d\alpha}$$

Since u_1 and u_2 in (13.16) are constants, the last two derivatives are zero.

where \mathcal{H} is the relative humidity. We can use the chain rule to expand further the derivatives in (13.17) to obtain

$$\frac{dw_v}{dT_0} = \frac{\varepsilon}{p} \frac{\partial T(p)}{\partial \Gamma} \frac{d\Gamma}{dT_0} \left[e_s(p) \frac{\partial \mathcal{H}(p)}{\partial T(p)} + \mathcal{H}(p) \frac{\partial e_s(p)}{\partial T(p)} \right]$$

where Γ is the atmospheric lapse rate (1.2). Using the Clausius-Clapeyron equation (4.21), we can write

$$\frac{dw_v}{dT_0} = w_s \frac{\partial T(p)}{\partial \Gamma} \frac{d\Gamma}{dT_0} \left[\frac{\partial \mathcal{H}(p)}{\partial T(p)} + \frac{\mathcal{H}(p) L_{lv}}{R_v T^2(p)} \right] \quad (13.18)$$

where w_s is the saturation mixing ratio (4.37). Incorporating (13.18) into (13.16), we obtain finally

$$f = G_o \frac{\partial F^{rad}}{\partial \mathcal{W}_v} \frac{1}{g} \int_0^{p_0} \left[w_s \frac{\partial T}{\partial \Gamma} \frac{d\Gamma}{dT_0} \left[\frac{\partial \mathcal{H}}{\partial T} + \frac{\mathcal{H} L_{lv}}{R_v T^2} \right] \right] dp \quad (13.19)$$

To illuminate the physics behind the water vapor feedback, consider the following simple example. If $\partial \mathcal{H} / \partial T_0 = 0$, we can simplify (13.19) to be

$$f = G_o \frac{\partial F^{rad}}{\partial \mathcal{W}_v} \frac{L_{lv}}{R_v g} \int_0^{p_0} \frac{\partial T}{\partial \Gamma} \frac{d\Gamma}{dT_0} \frac{w_v}{T^2} dp \quad (13.20)$$

where we have used $w_v = \mathcal{H} w_s$. If we assume a simple functional relationship for w_v , such as

$$w_v = w_{s0} \mathcal{H}_0 \left(\frac{p}{p_0} \right) = \mathcal{H}_0 \varepsilon \frac{e_s(T_0)}{p_0} \mathcal{H}_0 \left(\frac{p}{p_0} \right) \approx \frac{p}{p_0} a \exp(-b/T_0) \mathcal{H}_0^2$$

where

$$\mathcal{W}_v = \frac{1}{2g} \mathcal{H}_0^2 a \exp(-b/T_0)$$

where the constants a and b are easily determined from (4.31) and \mathcal{H}_0 is the surface air humidity. We can then write (13.20) as

$$f = G_o \frac{\partial F^{rad}}{\partial \mathcal{W}_v} \frac{L_{lv}}{R_v} \frac{2}{p_0^2} \mathcal{W}_v \int_0^{p_0} \frac{\partial T}{\partial \Gamma} \frac{d\Gamma}{dT_0} \frac{p}{T^2} dp \quad (13.21)$$

If we further assume that the lapse rate is constant with height in the atmosphere, we can write from (1.48)

$$T = T_0 \left(\frac{p}{p_0} \right)^{R_v \Gamma / g}$$

and

$$\frac{dT}{d\Gamma} = \frac{dT_0}{d\Gamma} \left(\frac{p}{p_0} \right)^{R_v \Gamma / g} + T_0 \left(\frac{p}{p_0} \right)^{R_v \Gamma / g} \frac{R_v}{g} \ln \frac{p}{p_0}$$

We can then evaluate the integral in (13.21) to obtain

$$f = G_o \frac{\partial F^{rad}}{\partial \mathcal{W}_v} \frac{L_{lv}}{R_v} 2\mathcal{W}_v \left[\frac{1}{T_0^2 \left(2 - \frac{R_v \Gamma}{g} \right)} + \frac{R_v}{g T_0} \frac{1}{\left(2 - \frac{R_v \Gamma}{g} \right)^2} \frac{d\Gamma}{dT_0} \right] \quad (13.22)$$

If the lapse rate remains constant, $d\Gamma/dT_0 = 0$, and we can write

$$f = G_o \frac{\partial F^{rad}}{\partial \mathcal{W}_v} \frac{L_{lv}}{R_v} \frac{2\mathcal{W}_v}{T_0^2 \left(2 - \frac{R_v \Gamma}{g} \right)} \quad (13.23)$$

which is a positive quantity since $\partial F^{rad}/\partial \mathcal{W}_v > 0$ and $R_v \Gamma / g < 2$ for all values of Γ . From (13.23), we can estimate that

$$\frac{1}{\mathcal{W}_v} \frac{\partial \mathcal{W}_v}{\partial T_0} = \frac{L_{lv}}{R_v} \frac{2}{T_0^2 \left(2 - \frac{R_v \Gamma}{g} \right)} \approx 7.7\%$$

The water vapor path increases with temperature by a fractional rate of about 7.7% K⁻¹ under standard atmospheric conditions. The rationale behind the simple expression (13.23) has dominated the thinking on water vapor feedback, whereby it is determined primarily by increased evaporation from the ocean surface according to the Clausius-Clapeyron relationship. However, some recent research has brought into question this simplified view of the water vapor feedback.

Variations of the lapse rate associated with a change in surface temperature, $d\Gamma/dT_0$ can alter the sign of the water vapor feedback. In the highly convective tropics, $d\mathcal{W}_v/dT_0$ is dominated by $d\Gamma/dT_0$, which is negative. Hence the lapse rate variation diminishes the water vapor

feedback in the tropics. At higher latitudes, the mid- and upper-troposphere has been simulated in climate models to warm less rapidly than the surface so that the lapse rate increases, and hence $d\Gamma/dT_0 > 0$. Therefore, the lapse rate variation acts to enhance the water vapor feedback in higher latitudes.

The net radiative flux is sensitive to vertical variations in the distribution of water vapor, even if there is no net change to \mathcal{W}_v . The net radiative flux is more sensitive to changes in water vapor amount in regions of the atmosphere where the water vapor mixing ratio is low, such as the upper troposphere (globally) and the lower troposphere in the polar regions. The relatively high sensitivity arises primarily from the infrared radiative transfer in the water vapor rotation band, at around 20 μm . Since low values of water vapor mixing ratio occur typically at low temperatures, the wavelength of maximum emission (3.21) occurs at longer wavelengths, and radiative transfer in the water vapor rotation band becomes increasingly important. Therefore the mechanisms controlling the humidity in these dry zones, particularly those that occur at cold temperatures, are of particular importance for understanding the water vapor feedback.

Two of these dry zones have been studied in detail, the upper tropical troposphere and the lower polar troposphere. In applying the type of feedback analysis described above, it must be remembered that this model represents the global energy budget, and care must be taken in using such a model to characterize regional responses. In applying expressions such as (13.20) and (13.23) to the examination of regional feedback processes, variations in large-scale dynamical transport may dominate the local thermodynamic processes in determining the sign and magnitude of the feedback.

13.3.1 Tropical upper troposphere

In the tropics, OLR is very sensitive to changes in upper tropospheric water vapor content. The lower tropospheric moisture content is very high, with a corresponding high water vapor emissivity. Therefore, small changes in lower tropospheric moisture content have little influence on either the local tropical outgoing longwave radiation, OLR, or the surface downwelling longwave flux, F_{00}^{LW} . The sign of the tropical water vapor feedback therefore depends on the sign of $d\mathcal{W}_v/dT_0$ in the upper troposphere.

The simple relationship in (13.17) associates a warmer surface with higher water vapor contents of the air above that surface. Even in the convectively-active tropics, a direct link between surface temperature and water vapor amount occurs only in the turbulent boundary layer, below about 700 hPa. Above the boundary layer, in the free troposphere, other less well-understood processes control the humidity of the air.

Figure 13.4 shows a histogram of relative humidity values as a function of atmospheric pressure, obtained from radiosonde observations in the tropical western Pacific. The levels below 700 hPa are moist with $\mathcal{H} = 70\text{--}90\%$, as would be expected for the turbulent boundary layer with the tropical ocean as a moisture source. In the layer between 500 and 250 hPa, much drier conditions exist, with a peak in the frequency distribution at $\mathcal{H} = 15\%$. At higher levels, the average humidity moistens to form a peak near $\mathcal{H} = 35\%$ just below the tropopause, which is typically near 100 hPa in the tropics.

The sharp decrease in \mathcal{H} above 700 hPa rules out the possibility of large-scale upward transport of water vapor from the boundary layer. The source of upper tropospheric moisture in the convectively-active regions of the tropics is most likely to be the vertical transport of condensed water and the subsequent convective detrainment. *Detrainment* is a process whereby air and cloud particles are transferred from the organized convective updraft to the surrounding atmosphere (the opposite of entrainment). Deep convection in the tropics detrains at a level just below the tropopause, accounting for the maxima in relative humidity at this level. Deep convective clouds are not the only convective process of importance in determining the tropical water vapor profile. The influence of the full range of convective clouds, particularly mesoscale convective complexes, are important in determining the vertical moisture distribution in convectively-active regions. Mesoscale convective systems contain convective cells of various depths and stages of development with detraining tops supplying moisture over the entire depth of the troposphere.

Deep convection in the tropics also generates widespread and often deep upper-level anvil clouds which generate precipitation. Some of the anvil precipitation evaporates into the subsaturated air below the cloud, often occurring at some distance away from the convective core. The outflow region is also a region of widespread compensating subsidence. Subsidence advects the water vapor downward, decreasing the upper tropospheric water vapor mixing ratio. Subsidence also decreases the relative humidity through compressional heating. Hence we have detrainment and evaporation of anvil precipitation acting to moisten the tropical environment, while compensating subsidence dries the tropical environment.

Lindzen (1990) has hypothesized that the tropical water vapor feedback is negative, whereby a warmer T_0 results locally in decreased upper tropospheric water vapor content. Such a negative relationship between T_0 and \mathcal{W}_v might arise from:

1. increased surface temperature producing deeper convection with higher, colder cloud tops, with relatively dry air being detrained in the upper troposphere;

2. a warmer atmosphere resulting in increased precipitation efficiency (warm rain process), resulting in the water vapor cycling through the atmosphere at relatively low altitudes, with less water transported to the upper troposphere.

The processes controlling the vertical mass flux in deep convection and precipitation efficiency are not well known for tropical mesoscale convective systems. It is not clear whether deep convection acts to dry or moisten the upper troposphere. Even more uncertain is how this will change in a warmer climate. The magnitude and sign of the local tropical water vapor feedback remains controversial. An additional difficulty is that an analysis of the local tropical thermodynamic water vapor feedback can be misleading, since advection is an important part of the moisture budget.

When determining water vapor feedback using a numerical climate model, the parameterizations of convection and precipitation processes (see Section 8.6) are crucial in determining the vertical distribution of water vapor, especially in the tropics. In view of the uncertainties in parameterization of these processes, the ubiquity of the positive water vapor feedback in the tropics found by these models should be questioned.

13.3.2 Polar troposphere

The second regional example of water vapor feedback considered here occurs in the wintertime polar regions. During winter, the polar troposphere is very stable (see Figure 8.17), due to strong radiative cooling of the surface. Because of this great stability, there is a lack of convective coupling between the surface and troposphere. Associated with the vertical temperature inversions are humidity inversions (see Section 8.4). Radiative cooling of the lower troposphere results in the formation of low-level clouds that are crystalline (diamond dust) at temperatures below about -15°C . Subsequent fallout of these ice crystals dehydrates the lower atmosphere, constraining the relative humidity so that it does not exceed the ice saturation value.

The process of diamond dust formation results in a positive value of $\partial\mathcal{H}/\partial T$ in (13.19), since the relative humidity is constrained not to exceed \mathcal{H}_i , the ice saturation value. Observations (Figure 13.5) show that the mean monthly relative humidity with respect to ice in the wintertime lower Arctic troposphere is $\mathcal{H}_i = 93\%$, for all air temperatures colder than about -10°C , so $\partial\mathcal{H}_i/\partial T = 0$. However, (4.35) and Table 4.4 imply that $\partial\mathcal{H}/\partial T > 0$ when $\partial\mathcal{H}_i/\partial T = 0$. Thus the additional positive term $\partial\mathcal{H}/\partial T$ in (13.19) contributes to a larger positive water vapor feedback in the polar regions than would be expected from the simple expression (13.21).

13.4 Cloud-radiation Feedback

Changes in cloud characteristics induced by a climate change would modify the radiative fluxes, thus altering the surface and atmospheric temperatures and further modify cloud characteristics. The feedback between surface temperature, clouds, and the Earth's radiation balance is referred to as the *cloud-radiation feedback*. The cloud-radiation feedback may be described using (13.8) as

$$f = G_o \left[\frac{\partial F^{rad}}{\partial A_c} \frac{dA_c}{dT_0} + \frac{\partial F^{rad}}{\partial T_c} \frac{dT_c}{dT_0} + \frac{\partial F^{rad}}{\partial \tau_c} \frac{d\tau_c}{dT_0} \right] \quad (13.24)$$

where F^{rad} is the net radiative flux, A_c is the cloud fraction, T_c is the cloud temperature, and τ_c is the cloud optical depth. The first two terms on the right-hand side of (13.24) comprise the cloud-distribution feedback, while the third term represents the cloud-optical depth feedback.

The cloud-radiation feedback is illustrated using a signal flow graph in Figure 13.6. A perturbation to the Earth's radiation balance modifies surface temperature and possibly surface albedo. Changes in surface temperature will modify fluxes of radiation and surface sensible and latent heat, which will modify the atmospheric temperature, humidity and dynamics. Modifications to the atmospheric thermodynamic and dynamic structure will modify cloud properties (*e.g.*, cloud distribution, cloud optical depth), which in turn modify the radiative fluxes. An understanding and correct simulation of the cloud-radiation feedback mechanism requires understanding of changes in: cloud fractional coverage and vertical distribution as the dynamics and vertical temperature and humidity profiles change; and changes in cloud water content, phase and particle size as atmospheric temperature and composition changes. The cloud-radiative feedback is generally regarded as one of the most uncertain aspects of global climate simulations.

In the following subsections, the individual derivatives in (13.24) are discussed.

13.4.1 Cloud-radiative effect

To the extent that the net radiative flux at the top of the atmosphere is linearly related to cloud fraction, the sensitivity term $\partial F^{rad}/\partial A_c$ in

(13.24) can be related to a parameter called the *cloud-radiative effect*², CF^{net}

$$\frac{\partial F^{rad}}{\partial A_c} dA_c \approx CF^{net} = F^{rad}(A_c) - F^{rad}(0) \quad (13.25)$$

(note that the radiative fluxes are defined to be positive downwards). The cloud-radiative effect is defined to be the actual radiative flux (which depends on cloud amount) minus the radiative flux for cloud-free conditions, all other characteristics of the atmosphere and surface remaining the same. The values of the cloud-radiative effect are negative for cooling and positive for warming. The cloud-radiative effect is most often defined in the context of the net radiative flux at the top of the atmosphere, F_{TOA}^{rad} , although the cloud-radiative effect can also be defined in the context of the surface radiative flux, F_{Q0}^{rad} . In addition, we can separate the cloud-radiative effect into longwave and shortwave components:

$$CF^{LW} = - [F^{LW}(A_c) - F^{LW}(0)] \quad (13.26a)$$

$$CF^{SW} = F^{SW}(A_c) - F^{SW}(0) \quad (13.26b)$$

where

$$CF^{net} = CF^{SW} + CF^{LW} \quad (13.26c)$$

The cloud-radiative effect provides information on the overall effect of clouds on radiative fluxes, relative to a cloud-free Earth. The cloud-radiative effect can be evaluated exactly using a radiative transfer model, where fluxes obtained from a calculation for a cloud-free but otherwise exactly similar atmosphere is subtracted from a calculation for the actual cloudy atmosphere. Determination of the cloud-radiative effect from satellite is accomplished by separating the clear from the cloudy observations. In spite of the simplicity of evaluating the cloud-radiative effect at the top of the atmosphere using satellite data, such evaluations are somewhat ambiguous. Ambiguities arise since the distinction between clear and cloudy regions is not always simple (particularly in polar regions) and because other characteristics of the atmosphere (*e.g.*, water vapor amount, atmospheric and surface temperature) change in cloudy versus clear conditions, even in the same location.

² The term “cloud forcing” is typically used to refer to the cloud-radiative effect. We believe that the word “force” is a misnomer for this effect.

Table 13.1 provides some estimates of the mean annual global cloud radiative forcing at the top of the atmosphere. Clouds reduce the longwave emission at the top of the atmosphere since they are emitting at a colder temperature than the Earth's surface. At the same time, clouds decrease the net shortwave radiation at the top of the atmosphere because clouds overlying the earth reflect more shortwave radiation than does the cloud-free earth-atmosphere. Because of the partial cancellation of these effects, the net cloud-radiative effect has a smaller magnitude than either the individual longwave or shortwave terms. Both satellite and model estimates agree that the net cloud-radiative effect at the top of the atmosphere is negative and that shortwave effect dominates, i.e. that clouds reduce the global net radiative energy flux into the planet by about 20 W m^{-2} .

Table 13.1. Estimates of the mean annual, globally averaged cloud radiative effect (W m^{-2}) at the top of the atmosphere derived from satellite observations and general circulation models.

Basis	Investigation	CF^{LW}	CF^{SW}	CF^{net}
satellite	Ramanathan et al (1989)	31	-48	-17
satellite	Ardanuy et al. (1991)	24	-51	-27
models	Cess and Potter (1987)	23 to 55	-45 to -75	-2 to -34

While clouds appear to have a net cooling effect on the global planetary radiation balance, there are regional and seasonal variations in the sign and magnitude of the cloud-radiative effect. The effect of an individual cloud on the local radiation balance depends on the cloud temperature and optical depth, as well as the insolation and characteristics of the underlying surface. For example, a low cloud over the ocean reduces substantially the net radiation at the top of the atmosphere, because it increases the planetary albedo while having little influence on the longwave flux at the top of the atmosphere. On the other hand, a high thin cloud can greatly decrease the outgoing longwave fluxes while having little influence on the solar radiation, therefore increasing the net radiation at the top of the atmosphere.

13.4.2 Cloud distribution feedback

Changes in cloud fraction and in the vertical distribution of clouds induced by a climate change could modify the radiative fluxes and further modify cloud properties. From (13.24), the cloud-distribution feedback can be written as

$$f = G_o \left[\frac{\partial F^{rad}}{\partial A_c} \frac{dA_c}{dT_0} + \frac{\partial F^{rad}}{\partial T_c} \frac{dT_c}{dT_0} \right] \quad (13.27)$$

The general behavior of $\partial F^{rad}/\partial A_c$ and $\partial F^{rad}/\partial T_c$ has been described in subsection 13.4.1, in the context of the cloud-radiative effect. Determination of the terms dA_c/dT_0 and dT_c/dT_0 are far more difficult, since it requires understanding how cloud amount and its vertical distribution will vary in response to an altered value of T_0 .

Simulations using global climate models of a doubled carbon dioxide (greenhouse warming) scenario generally show:

- cloud cover overall reduced at mid- and low-latitudes
- increased cloudiness near the tropopause at middle and high latitudes
- increased cloudiness near the surface at middle and high latitudes

Most general circulation models produce a positive cloud-distribution feedback, resulting from a decrease of low-level cloudiness (with a large albedo but warm temperature) and an increase in high clouds (with low temperature and a smaller albedo).

In addition to changes in T_c arising from changes in the altitude of the cloud, changes in T_c arise from changing atmospheric temperatures. Climate models generally predict a warming of the troposphere in a scenario with increased greenhouse gases.

An additional aspect of the cloud-distribution feedback is the temporal distribution of clouds over the diurnal cycle. Shifting 10% of the nighttime cloud cover to daytime produces an effect that is large enough to offset the effects of doubling atmospheric CO_2 . This is a consequence of the delicate balance between shortwave effects (confined to daytime) and longwave effects.

13.4.2 Cloud optical depth feedback

The *cloud optical depth feedback* is written from (13.8) as

$$f = G_o \frac{\partial F_{Q_0}^{rad}}{\partial \tau_c} \frac{d\tau_c}{dT_0} \quad (13.28)$$

The partial derivatives $\partial F^{rad}/\partial \tau_c$ have the same sign as the derivative $\partial F^{rad}/\partial A_c$: the partial derivative is negative for F^{SW} and positive for F^{LW} , with similar variations for changes in cloud height. Assuming that the cloud distribution remains the same, if $d\tau_c/dT_0 > 0$, then the cloud optical depth feedback will be negative, since $\partial F^{rad}/\partial \tau_c < 0$.

The derivative $d\tau_c/dT_0$ can be interpreted by using the chain rule. Since the cloud optical depth is a function of the amount of condensed

water, its phase, and the size of the particles, we can use (8.12) to expand $d\tau_c/dT_0$ as

$$\frac{d\tau_c}{dT_0} = \frac{3}{2} \left(\frac{1}{r_{el}\rho_l} \frac{d\mathcal{W}_l}{dT_0} + \frac{1}{r_{ei}\rho_i} \frac{d\mathcal{W}_i}{dT_0} - \frac{1}{r_{el}^2} \frac{dr_{el}}{dT_0} - \frac{1}{r_{ei}^2} \frac{dr_{ei}}{dT_0} \right) \quad (13.29)$$

where r_{el} and r_{ei} are the effective radii for liquid and ice particles. To assess the cloud optical depth variation with surface temperature, we next consider the individual terms in (13.29).

The derivative $d\mathcal{W}_l/dT_0$ has been hypothesized to be positive, whereby a warmer (and presumably moister) lower atmosphere would increase the liquid water content of clouds. To assess this hypothesis, we consider a single layer liquid water cloud and expand the derivative $d\mathcal{W}_l/dT_0$ using the definition of the liquid water path (8.6)

$$\frac{d\mathcal{W}_l}{dT_0} = \frac{d}{dT_0} \frac{1}{g} \int_{p_t}^{p_b} w_l dp = \frac{1}{g} \int_{p_t}^{p_b} \frac{dw_l}{dT_0} dp + \frac{1}{g} \left[w_{lt} \frac{dp_t}{dT_0} - w_{lb} \frac{dp_b}{dT_0} \right] \quad (13.30)$$

where w_l is the liquid water mixing ration and p_t and p_b are, respectively, the cloud top and base pressures. The second term on the right-hand side of (13.30) arises from the variation of p_t and p_b with T_0 (see the footnote in Section 13.3). If we assume that w_l is constant within the cloud, we have $w_l = g\mathcal{W}_l/(p_b - p_t)$ and therefore can write (13.30) as

$$\frac{d\mathcal{W}_l}{dT_0} = \frac{d}{dT_0} \frac{1}{g} \int_{p_t}^{p_b} w_l dp = \frac{1}{g} \int_{p_t}^{p_b} \frac{dw_l}{dT_0} dp + \mathcal{W}_l \frac{d \ln(p_b - p_t)}{dT_0} \quad (13.31)$$

If we assume that the cloud forms in saturated adiabatic ascent, the integral on the right-hand-side of (13.31) can be expanded as

$$\frac{1}{g} \int_{p_t}^{p_b} \frac{dw_l}{dT_0} dp = D \frac{\partial \mathcal{W}_{l,ad}}{\partial T_0} + \mathcal{W}_{l,ad} \frac{\partial D}{\partial T_0} \quad (13.32)$$

where the term $\mathcal{W}_{l,ad}$ is the adiabatic liquid water path defined in Section 8.2. The term D represents the cloud water dilution relative to the adiabatic liquid water path, which arises from entrainment, precipitation, and conversion to the ice phase. We can therefore write (13.31) as

$$\frac{d\mathcal{W}_l}{dT_0} = D \frac{\partial \mathcal{W}_{l,ad}}{\partial T_0} + \mathcal{W}_{l,ad} \frac{\partial D}{\partial T_0} + \mathcal{W}_l \frac{d \ln(p_t - p_b)}{dT_0} \quad (13.33)$$

The term $\partial \mathcal{W}_{lad} / \partial T_0$ is positive as long as the lower atmospheric temperature increases with increasing surface temperature, which is a reasonable assumption. The sign of the term $\partial D / \partial T_0$ depends on issues such as whether the precipitation efficiency in a warmer climate will increase and whether the clouds will be more convective or stratiform in a warmer climate and thus modify dilution by entrainment. The term $\partial D / \partial T_0$ has a negative component if the phase of mid-level clouds is more likely to be liquid (rather than crystalline) in a warmer environment. The last term on the right-hand side of (13.33) arises from a possible variation of cloud depth with changing surface temperature; the sign of this term is unknown. Although the adiabatic liquid water path in the lower atmosphere is expected to increase in a warmer climate, the sign of $\partial \mathcal{W}_{lad} / \partial T_0$ remains unknown because of uncertainties in processes that control cloud depth, entrainment, and precipitation efficiency, which vary with cloud type.

A similar analysis can be done for the term $d\mathcal{W}_i/dT_0$. To interpret this term, we consider a single-layer ice cloud in the upper troposphere and expand the derivative $d\mathcal{W}_i/dT_0$

$$\frac{d\mathcal{W}_i}{dT_0} = \frac{1}{g} \int_{p_t}^{p_b} \frac{dw_i}{dT_0} dp + \mathcal{W}_i \frac{d \ln(p_t - p_b)}{dT_0} \quad (13.34)$$

where w_i is the ice-water mixing ratio. The integral on the right-hand-side of (13.34) can be expanded as

$$\frac{1}{g} \int_{p_t}^{p_b} \frac{dw_i}{dT_0} dp = \frac{1}{g} \int_{p_t}^{p_b} \frac{\partial w_i}{\partial T_c} \frac{dT_c}{dT_0} dp \quad (13.35)$$

where T_c is the cloud temperature. We can therefore write (13.34) as

$$\frac{d\mathcal{W}_i}{dT_0} = \frac{1}{g} \int_{p_t}^{p_b} \frac{\partial w_i}{\partial T_c} \frac{dT_c}{dT_0} dp + \mathcal{W}_i \frac{d \ln(p_t - p_b)}{dT_0} \quad (13.36)$$

Observations such as those shown in Figure 13.7 show that the derivative $dw_i/dT_c > 0$. Simulations from climate models indicate that upper tropospheric temperatures increase with a surface warming, so that $dT_c/dT_0 > 0$ and the first term on the right-hand side of (13.36) is positive. The sign of the second term on the right-hand side of (13.36) is unknown. Variations in cirrus cloud depth with a surface warming depend, in complex ways, on changes to deep convection and the strength of mid-latitude frontal systems.

Several mechanisms have been suggested for changes in cloud particle size in a global warming scenario. Recall the definition of r_e for a distribution of spherical particles (8.13):

$$r_e = \frac{\int_0^\infty r^3 n(r) dr}{\int_0^\infty r^2 n(r) dr}$$

The effective radius can vary with the amount of condensed water and the number of condensed particles. We can therefore write

$$\frac{dr_{el}}{dT_0} = \frac{\partial r_{el}}{\partial w_l} \frac{\partial w_l}{\partial T_{cl}} \frac{dT_{cl}}{dT_0} + \frac{\partial r_{el}}{\partial N_l} \frac{dN_l}{dT_0} \quad (13.37a)$$

$$\frac{dr_{ei}}{dT_0} = \frac{\partial r_{ei}}{\partial w_i} \frac{\partial w_i}{\partial T_{ci}} \frac{dT_{ci}}{dT_0} + \frac{\partial r_{ei}}{\partial N_i} \frac{dN_i}{dT_0} \quad (13.37b)$$

where T_{cl} is the temperature of the liquid cloud, T_{ci} is the temperature of the ice cloud, N_l is the number concentration of water drops, and N_i is the number concentration of ice particles.

The partial derivatives $\partial r_e / \partial w$ in (13.37a) and (13.37b) are positive; assuming that N remains constant, an increase in the amount of condensed water implies an increase in particle size. The derivatives $\partial w / \partial T_c$ are also positive, as discussed previously in this section. Furthermore, as described in the discussion regarding the dW/dT_0 terms, it was shown that $dT_c/dT_0 > 0$. Hence the first term is positive on the right-hand sides of (13.37a) and (13.37b).

If the number concentration increases, and all other things remain constant (such as liquid and ice water mixing ratio), then the effective radius will decrease, so that $\partial r_e / \partial N < 0$. Changes in droplet and ice particle concentrations, N_l and N_i , could arise from:

- changes in the concentrations of cloud condensation nuclei (CCN) and ice-forming nuclei (IFN);
- changes in the rate of entrainment that evaporate or sublimate cloud particles;
- changes in the efficiency of precipitation which would alter the number of cloud particles that fall out of the cloud; and
- changes in the phase of precipitation due to freezing or melting, where $dN_l = -dN_i$.

For there to be a feedback associated with N , there must be some relation between N and T_0 . An increase in the number of CCN can arise

from anthropogenic pollution, which is an external climate forcing. An internal source of CCN has been hypothesized to occur via the oxidation of dimethylsulfide (DMS), which is emitted by phytoplankton in seawater. Therefore, DMS from the oceans may determine the concentrations and size spectra of cloud droplets. If it is assumed that the DMS emissions increase with increasing ocean temperature, there would be an increase in atmospheric aerosol particles and $dN_i/dT_0 > 0$. However, the increase of DMS emissions with increasing ocean temperature has not been verified from observations. Additionally, the factors which most enhance biological productivity are sunlight and nutrients; incoming sunlight would be depleted by additional aerosols, which might reduce the production of DMS.

Additional relationships between N and T_0 might arise from changes in cloud type in an altered climate, whereby an increase in convective clouds would increase both entrainment and precipitation; both processes would decrease N . An increase in droplet concentration may in itself reduce precipitation efficiency and hence increase the lifetime (cloud fraction) and optical depth of the cloud (Albrecht 1989). Warmer air temperature at heights where atmospheric temperature ranges between about 0 and -15°C would result in an increasing amount of liquid relative to ice phase clouds (Mitchell *et al.*, 1989). Since clouds with ice in them are more likely to form precipitation-sized particles, the cloud water content would increase as the atmosphere warms.

In summary, the cloud-optical depth feedback is very complex. Climate models that include at least some of the cloud microphysical processes involved in the cloud-optical depth feedback generally find that this is a negative feedback. However, the sign and magnitude of the feedback depends on the cloud parameterizations that are used in the model, introducing substantial uncertainty into the estimation.

13.5 Snow/Ice-albedo Feedback

The possible importance of high-latitude snow and ice for climate change has been recognized since the 19th century. It has been hypothesized that when climate warms, snow and ice cover will decrease, leading to a decrease in surface albedo and an increase in the absorption of solar radiation at the Earth's surface, which would favor further warming. The same mechanism works in reverse as climate cools. This climate feedback mechanism is generally referred to as the *snow/ice-albedo feedback*, which is a positive feedback mechanism. The ice-albedo feedback has proven to be quite important in simulations of global warming in response to increased greenhouse gas concentrations.

The snow/ice albedo feedback can be separated into the feedbacks associated with land snow/ice and sea ice. Additionally, the land and sea

ice albedo feedbacks each may be separated into a feedback associated with the changing horizontal extent of the sea ice and a feedback associated with local processes in the snow or ice pack (*e.g.*, processes related to snow and melt ponds) (Figure 13.8).

In the context of a surface energy balance model, we can write the following expression for the snow/ice albedo feedback mechanism over the ocean:

$$f = G_o \frac{\partial F_{Q0}^{rad}}{\partial \alpha_0} \frac{d\alpha_0}{dT_0} \quad (13.38)$$

where by definition of the surface albedo, α_0 , we have $\partial F_{Q0}^{rad} / \partial \alpha_0 < 0$. To date, most of the research on ice albedo feedback has focused on the terms

$$\frac{d\alpha_0}{dT_0} = \frac{dA_i}{dT_0} \alpha_i + \frac{dA_L}{dT_0} \alpha_L$$

where the subscript i denotes ice, the subscript L denotes open water, and A is the fractional area coverage. In a simple model where the surface is either ice-covered or open water, then $dA_i = -dA_L$, so we can write

$$\frac{d\alpha_0}{dT_0} = \frac{dA_i}{dT_0} (\alpha_i - \alpha_L)$$

Since the area coverage of sea ice will decrease in a warmer climate ($dA_i/dT_0 < 0$) and $\alpha_i > \alpha_L$, the term $d\alpha_0/dT_0 < 0$, and from (13.38), we have $f > 0$.

As discussed in Section 10.5, the surface albedo of an ice covered ocean is quite complex, including contributions from melt ponds, snow-covered ice, open water in leads, and bare ice. To assess the contribution of each of these different surface types to the albedo feedback (Figure 13.8), we can write the surface snow/ice albedo as the fractional-area-weighted sum of the albedos of the individual surface types that characterize ice-covered oceans:

$$\alpha_0 = A_i \alpha_i + A_L \alpha_L + A_P \alpha_P + A_s \alpha_s \quad (13.39)$$

where A denotes the fractional area/time coverage of the individual surface types and the subscripts i , L , P , and s denote, respectively, bare ice, open water in leads, melt ponds, and snow. Differentiating (13.39) with respect to T_0 yields

$$\begin{aligned} \frac{d\alpha_0}{dT_0} = & A_i \frac{d\alpha_i}{dT_0} + \frac{dA_i}{dT_0} \alpha_i + A_L \frac{d\alpha_L}{dT_0} + \frac{dA_L}{dT_0} \alpha_L + \\ & + A_P \frac{d\alpha_P}{dT_0} + \frac{dA_P}{dT_0} \alpha_P + A \frac{d\alpha_S}{dT_0} + \frac{dA_S}{dT_0} \alpha_S \end{aligned} \quad (13.40)$$

Analogously to the cloud-radiation feedback, we can divide the ice-albedo feedback into an ice-area-distribution feedback and a surface-optical properties feedback.

Consider first the terms in (13.40) that include dA/dT_0 , which comprises the ice-area-distribution feedback (outer loop in Figure 13.8)

$$\frac{dA_j}{dT_0} \alpha_j \equiv \frac{dA_i}{dT_0} \alpha_i + \frac{dA_L}{dT_0} \alpha_L + \frac{dA_P}{dT_0} \alpha_P + \frac{dA_S}{dT_0} \alpha_S \quad (13.41)$$

where the subscript j on the left-hand side of (13.41) is simply an index. Table 13.2 summarizes mid-summer values of α_j (Table 10.1) along with the expected signs of dA_j/dT_0 . It seems reasonable to expect that $dA_S/dT_0 < 0$, $dA_L/dT_0 > 0$, and $dA_i/dT_0 < 0$, since a warmer climate would likely be associated with more open water and less snow and bare ice. In a warmer climate as the ice thins, melt ponds may become “melt holes” as the ponds melt through the ice, decreasing A_P and increasing A_L . In a warmer climate, the area of the high-albedo surfaces will decrease and the area of the low-albedo surfaces will increase; hence, $\alpha dA/dT_0 < 0$.

Table 13.2 Magnitude and/or sign of the terms in (13.41)

Ice type	Summertime	
	albedo	dA/dT_0
Bare ice	0.56	< 0
Open water	0.10	> 0
Melt ponds	0.25	< 0
Snow	0.77	< 0

Next consider the terms in (13.40) that include $A d\alpha/dT_0$, which comprise the surface-optical properties feedback (inner loop in Figure 13.8):

$$A_j \frac{d\alpha_j}{dT_0} \equiv A_i \frac{d\alpha_i}{dT_0} + A_L \frac{d\alpha_L}{dT_0} + A_P \frac{d\alpha_P}{dT_0} + A_S \frac{d\alpha_S}{dT_0} \quad (13.42)$$

where again, j is an index.

The albedo of bare ice depends on ice thickness and the age of the sea ice. We can therefore write

$$\frac{d\alpha_i}{dT_0} = \frac{dh_i}{dT_0} \left[\frac{\partial\alpha_i}{\partial h_i} + \frac{\partial\alpha_i}{\partial y_i} \frac{\partial y_i}{\partial h_i} \right] \quad (13.43)$$

where the term y denotes the age of the ice and h_i is ice thickness. Since thick ice is associated with colder surface temperatures (Figure 10.8), $dh_i/dT_0 < 0$. If the ice thickness is less than 2 m, the albedo is influenced by the underlying ocean, and thus $\partial\alpha_i/\partial h_i > 0$. Old ice has air bubbles which increase in concentration with ice age; hence older ice has a higher surface albedo (Section 10.5) and $\partial\alpha_i/\partial y_i > 0$. Since ice thickness generally increases with ice age, $\partial y_i/\partial h_i > 0$. Therefore, $A_i d\alpha_i/dT_0 < 0$. In (13.42), the term $d\alpha_l/dT_0 = 0$, since there is no reason for the albedo of open water to vary with surface temperature. The albedo of melt ponds decreases with increasing melt pond depth. Thicker ice can support deeper melt ponds. Hence we can write

$$\frac{d\alpha_P}{dT_0} = \frac{\partial\alpha_i}{\partial h_P} \frac{\partial h_P}{\partial h_i} \frac{dh_i}{dT_0} \quad (13.44)$$

Since pond albedo decreases with increasing pond depth, we have $\partial\alpha_i/\partial h_P < 0$. We have also seen that $dh_i/dT_0 < 0$. However, the variation of pond depth with ice thickness is not straightforward. On one hand, thicker ice can support deeper melt ponds. On the other hand, as ponds deepen in thin ice, further deepening of the pond may be accelerated as the pond albedo lessens due to the influence of the underlying ocean, becoming “melt holes” as they melt through the ice, and the pond depth becomes undefined. The albedo of snow depends on snow depth and snow age. Deeper snow and more frequent snowfalls are associated with a higher value of surface albedo. If a warmer climate (associated with higher T_0) is also associated with higher snowfall amount in the polar regions, then $d\alpha_s/dT_0 > 0$, but the sign of this term must be regarded as uncertain, since the characteristics of snowfall in an altered climate are not known.

To summarize the preceding analysis of snow/ice-albedo feedback, a negative value of $d\alpha_0/dT_0 = \alpha_j dA_j/dT_0 + A_j d\alpha_j/dT_0$ will give a positive value of the snow/ice albedo feedback in (13.38), since $\partial F_{\text{net}}^{\text{rad}}/\partial\alpha_0 < 0$. The sign of $\alpha_j dA_j/dT_0$ is unambiguously negative, although the sign of $A_j d\alpha_j/dT_0$ is less certain and may depend critically on whether snowfall over sea ice increases in a warmer climate. While the overall sign of the snow/ice-albedo feedback is not in doubt, its magnitude in climate models depends on the details of the snow and sea ice model parameterizations, such as snow albedo, melt ponds, sea ice dynamics, etc.

An additional factor to consider in the context of the snow/ice albedo feedback is the influence of clouds on the surface albedo of snow and ice. As described in Section 10.5, the broadband surface albedo of snow and ice can be significantly higher under cloudy skies than under clear skies, because clouds deplete the incoming solar radiation in the infrared portion of the spectrum and change the direct beam radiation to diffuse radiation. If the local cloud-radiation feedback is nonzero, then an additional component to the snow/ice albedo feedback must be considered.

13.6 Thermodynamic Control of the Tropical Ocean Warm Pool

In Section 11.3.1, the tropical ocean warm pool was discussed. Skin temperature is observed to be less than 34°C, while ocean temperatures measured at a depth of 0.5 m typically do not exceed 32°C. Geochemical studies of paleoclimatic data (*Crowley and North, 1991*) suggest that the maximum annually-averaged equatorial sea surface temperatures have not exceeded about 30°C during warm climatic episodes. However, there is controversy about the paleoclimatic situation during the last ice age (*Webster and Stretten, 1978*), where the warm pool may have been as cold as 24°C. Nevertheless, it appears that the equatorial sea surface temperature is remarkably insensitive to global climatic forcing, in contrast to the pronounced sensitivity of mid and high latitudes (*e.g.*, ice ages). It appears that negative feedbacks are acting to stabilize the tropical ocean surface temperature. The nature of the negative feedbacks in this region continues to be hotly debated.

The simple planetary energy balance model described in Section 13.2 is predicated upon the principle that when averaged over the entire Earth and over an annual cycle, the net incoming solar radiation at the top of the atmosphere is equal to the outgoing longwave radiation balance at the top of the atmosphere. This assumption results in elimination of the term ΔF_{TOA}^{rad} in (13.9). To consider the energy balance at the top of the atmosphere for a region, the term ΔF_{TOA}^{rad} cannot be neglected since advection of heat into or out of the region will change the local energy balance at the top of the atmosphere.

Hence, in examining regional climate feedbacks, it is more fruitful to conduct the feedback analysis using a surface energy balance model, whereby the surface energy balance is written from (9.1) as

$$F_{Q0}^{net} - F_{Q0}^{adv} - F_{Q0}^{ent} = F_{Q0}^{rad} + F_{Q0}^{SH} + F_{Q0}^{LH} + F_{Q0}^{PR}$$

The sea surface temperature is determined by a balance between ocean heat transports and surface energy fluxes. For simplicity in the following

discussion, the distinction between the skin sea surface temperature, T_0 , and the ocean mixed layer temperature, T_m , is ignored, and it is assumed that $T_0 = T_m$. (see section 11.2 to recall the distinction between T_0 and T_m .) From (13.8), we can write the feedback for a surface energy balance model as

$$f = \mathcal{G}_o \sum_j \frac{\partial F_{Q0}^{net}}{\partial I_j} \frac{dI_j}{dT_0} \quad (13.45)$$

Incorporating (9.1) into (13.45), we can write

$$f = \mathcal{G}_o \sum_j \left[\frac{\partial F_{Q0}^{rad}}{\partial I_j} \frac{dI_j}{dT_0} + \frac{\partial F_{Q0}^{SH}}{\partial I_j} \frac{dI_j}{dT_0} + \frac{\partial F_{Q0}^{LH}}{\partial I_j} \frac{dI_j}{dT_0} + \frac{\partial F_{Q0}^{PR}}{\partial I_j} \frac{dI_j}{dT_0} + \frac{\partial F_{Q0}^{adv}}{\partial I_j} \frac{dI_j}{dT_0} + \frac{\partial F_{Q0}^{ent}}{\partial I_j} \frac{dI_j}{dT_0} \right] \quad (13.46)$$

The surface radiative flux feedbacks

$$f = \mathcal{G}_o \sum_j \frac{\partial F_{Q0}^{rad}}{\partial I_j} \frac{dI_j}{dT_0} \quad (13.47)$$

depend upon all of the internal variables discussed in Sections 13.3 and 13.4: water vapor, lapse rate, cloud fractional area, cloud temperature, and cloud optical depth. Hence we can write (13.47) as

$$f = \mathcal{G}_o \left[\frac{\partial F_{Q0}^{rad}}{\partial W_v} \frac{dW_v}{dT_0} + \frac{\partial F_{Q0}^{rad}}{\partial \Gamma} \frac{d\Gamma}{dT_0} + \frac{\partial F_{Q0}^{rad}}{\partial A_c} \frac{dA_c}{dT_0} + \frac{\partial F_{Q0}^{rad}}{\partial T_c} \frac{dT_c}{dT_0} + \frac{\partial F_{Q0}^{rad}}{\partial \tau_c} \frac{d\tau_c}{dT_0} \right] \quad (13.48)$$

In contrast to the tropical water vapor feedback on the planetary energy balance (section 13.3.1), the tropical water vapor feedback on the surface energy balance is quite straightforward. Because the water vapor content of the tropical atmospheric boundary layer is so high, the longwave flux at the surface shows little variation with the amount of water vapor, so that F_{Q0}^{rad} is relatively insensitive to variation in W_v . The value of F_{Q0}^{rad} is, however, quite sensitive to variations cloud properties. Again, because the water vapor content of the tropical atmospheric boundary layer is so high, the longwave flux at the surface F_{Q0}^{LW} is insensitive to variations in cloud characteristics. However, the shortwave flux at the surface F_{Q0}^{SW} is quite sensitive to variations in cloud fraction where $\partial F_{Q0}^{rad}/\partial A_c \approx \partial F_{Q0}^{SW}/\partial A_c < 0$. The term $\partial F_{Q0}^{rad}/\partial \tau_c$ is also positive. As discussed in Section 13.5, determination of dA_c/dT_0 and $d\tau_c/dT_0$ depends not only on local thermodynamic processes but also on large-scale dynamical processes.

Since the surface sensible heat flux over the tropical ocean is an order of magnitude smaller than the latent heat flux, here we consider

only the latent heat flux feedback (although the arguments are easily extended to include the sensible heat flux). The feedback associated with the latent heat flux is written from (13.8) as

$$f = G_o \sum_j \frac{\partial F_{Q0}^{LH}}{\partial I_j} \frac{dI_j}{dT_0} \quad (13.49)$$

From Section 9.1.2, the surface latent heat flux is determined to be

$$F_{Q0}^{LH} = \rho L_{iv} C_{DE} u_a (q_{va} - q_{v0})$$

and hence $F_{Q0}^{LH}(u_a, \Delta q, C_{DE})$ where $\Delta q = q_{v0} - q_{va}$. We can therefore expand (13.49)

$$\begin{aligned} f &= G_o \left[\frac{\partial F_{Q0}^{LH}}{\partial u_a} \frac{du_a}{dT_0} + \frac{\partial F_{Q0}^{LH}}{\partial \Delta q} \frac{d\Delta q}{dT_0} + \frac{\partial F_{Q0}^{LH}}{\partial C_{DE}} \frac{dC_{DE}}{dT_0} \right] \\ &\approx G_o \rho L_{iv} \left[C_{DE} \Delta q \frac{du_a}{dT_0} + C_{DE} u_a \frac{d\Delta q}{dT_0} \right] \end{aligned} \quad (13.50)$$

where the term dC_{DE}/dT_0 is ignored since it is estimated to be much smaller than the other terms. The individual terms in (13.50) have been evaluated using surface observations in the tropical Pacific Ocean (Zhang and McFadden, 1995). Typical values in the warm pool are $u_a = 5 \text{ m s}^{-1}$, $\Delta q = 6 \text{ g kg}^{-1}$, and $C_{DE} = 1.1 \times 10^{-3}$. It was shown that $d\Delta q/dT_0 > 0$, while $du_a/dT_0 < 0$. Wind speed dependence of the surface latent heat flux dominates for $T_0 > 301 \text{ K}$, while the humidity dependence dominates for $T_0 < 301 \text{ K}$. The decrease in surface latent heat flux at high surface temperatures is hypothesized to arise from the following mechanism: high surface temperature \rightarrow increased instability and convection \rightarrow increased large-scale low-level convergence \rightarrow weaker surface wind \rightarrow lower latent heat flux. In interpreting the magnitudes and signs of these derivatives, it should be kept in mind that an apparent empirical relationship between wind speed and humidity with T_0 is no guarantee that the primary factor giving rise to changes in wind speed or humidity is T_0 . Wind speed and T_0 may appear to be related because both fields are related to a third and much more dominant factor, such as the large-scale coupled atmosphere-ocean circulation, which is controlled largely by the horizontal gradient in T_0 rather than the value of T_0 itself.

The feedback associated with the sensible heat flux of rain

$$f = G_o \sum_j \frac{\partial F_{Q0}^{PR}}{\partial I_j} \frac{dI_j}{dT_0} \quad (13.51)$$

is believed to be smaller than the other terms in (13.46), since the long-term average magnitude of F_{Q0}^{PR} is about 2% of the value of F_{Q0}^{LH} . A change of F_{Q0}^{PR} with surface temperature might arise from a change in the amount of precipitation in an altered climate.

From (11.4), the heat flux from entrainment at the base of the ocean mixed layer, F_{Q0}^{ent} , can be written as

$$F_{Q0}^{ent} = \rho c_p u_e \Delta T$$

where u_e is the entrainment velocity at the base of the mixed layer and the term ΔT represents the jump in temperature across the base of the mixed layer. Recall from (11.6b) that the entrainment velocity is given by

$$u_e = \frac{c_1 u_*^3 - c_2 F_{B0} h_m}{h_m (\alpha g \Delta T - \beta g \Delta s)}$$

The feedback associated with entrainment can therefore be written as

$$\begin{aligned} f &= G_o \left[\frac{\partial F_{Q0}^{ent}}{\partial \Delta T} \frac{d\Delta T}{dT_0} + \frac{\partial F_{Q0}^{ent}}{\partial u_*^3} \frac{du_*^3}{dT_0} + \frac{\partial F_{Q0}^{ent}}{\partial F_{B0}} \frac{dF_{B0}}{dT_0} + \frac{\partial F_{Q0}^{ent}}{\partial h_m} \frac{dh_m}{dT_0} + \frac{\partial F_{Q0}^{ent}}{\partial \Delta s} \frac{d\Delta s}{dT_0} \right] \\ &\approx \frac{\rho c_p}{h_m \alpha g \Delta T} G_o \left[(c_1 u_*^3 - c_2 F_{B0} h_m) \frac{d\Delta T}{dT_0} + \Delta T c_1 \frac{du_*^3}{dT_0} - \Delta T c_2 h_m \frac{dF_{B0}}{dT_0} - \Delta T c_1 u_*^3 \frac{dh_m}{dT_0} \right] \end{aligned} \quad (13.52)$$

The term Δs has been ignored since there is not a strong halocline in the tropics, and $\Delta T > 0$ in the tropics. The feedback associated with entrainment depends on a complex interplay between surface momentum and buoyancy fluxes. Accumulation of buoyancy in the warm pool region alters the sensitivity of the sea surface temperature to wind forcing. When the mixed layer is shallow, entrainment cooling is more easily initiated. As heat and freshwater accumulate in the warm pool the threshold wind speed and duration of entrainment cooling increases, therefore rendering the mixed layer less sensitive to wind mixing.

The significance of the term F_{Q0}^{adv} can be explained as follows. If T_0 in the warm pool increases, both the east-west and meridional temperature gradients will increase. These gradients in upper ocean temperature generate increased transport of heat away from the warm pool. The meridional transport of heat away from the equatorial warm pool induces increased equatorial upwelling that cools the warm pool

mixed layer. Heat that accumulates in the tropical western Pacific is exported in El Niño conditions towards the east, reducing upwelling in the central and eastern Pacific. Hence, the tropical ocean circulation moves heat to where the ocean more readily loses it to the atmosphere.

In summary, the largest terms involved in the tropical ocean warm pool feedback appear to be associated with solar radiation, the surface latent heat flux, mixed-layer entrainment, and oceanic advection processes. The separation of these effects based on empirical studies alone is extremely difficult because all contributing factors are operating simultaneously and only total changes are observed. To determine whether the relationships inferred from the short-term variability may be extrapolated to longer-term climate changes or used to assess model feedbacks operating in climate change experiments, one has to estimate the dynamical dependence of relationships between the sea surface temperature, clouds, radiation, and processes that control the depth and heat content of the ocean mixed layer. Feedback hypotheses for the warm pool can only be tested fully by models of the coupled ocean-atmosphere system, once these models have demonstrated sufficient realism.

13.7 High-latitude Ocean Feedbacks

The global ocean thermohaline circulation was described in Section 11.6, whereby large-scale overturning is driven by both buoyancy and mechanical forces generated in high-latitude oceans. The response of the ocean thermohaline circulation to perturbations is determined by four major feedbacks between the thermohaline circulation and the high-latitude temperature and salinity fields (Figure 13.9).

Consider an equilibrium situation where a positive perturbation to the freshwater flux (*e.g.*, excess precipitation or sea ice melt) is imposed at high latitudes. A decrease in salinity corresponds to a decrease in density, which diminishes the sinking motion and the thermohaline circulation. The weakening of the thermohaline circulation reduces the poleward transport of relatively salty water from lower latitudes, which further decreases the polar salinity (loop 1 in Figure 13.9), which is a positive feedback.

At the same time, the decreased strength of the thermohaline circulation also reduces the northward heat transport, increasing the high-latitude surface density, which in turn intensifies the high-latitude convection and hence the overturning circulation (loop 2 in Figure 13.9), and hence is a negative feedback. This negative feedback partially compensates the positive feedback associated with salinity, but the compensation is not complete and the positive salinity feedback dominates.

Diminished overturning leads to lower surface temperatures, which results in reduced evaporation (loop 3 in Figure 13.9). If all of the evaporated water returns to the ocean locally in the form of precipitation, then there is no net effect and loop 3 is inactive. If precipitation falls outside the region of evaporation, then the feedback in loop 3 is positive. Lower surface temperature also results in increased sea ice formation, which increases the density and hence the thermohaline circulation.

A further result of decreased high latitude surface temperature is that the meridional atmospheric circulation is enhanced by the stronger meridional surface temperature gradient, resulting in increased northward transport of atmospheric heat and moisture, which increases precipitation and decreases the high latitude surface ocean density (loop 4 in Figure 13.9).

Given these feedbacks, what is the stability and variability of the thermohaline circulation? Climate stability can be analyzed reliably only if all important feedbacks are represented accurately in a climate model. In spite of deficiencies in current climate models, useful sensitivity studies can be conducted even with relatively simple models. In models where the haline feedback (loop 1) dominates, multiple equilibrium states are possible. Alternate equilibrium states that have been found include: a conveyor-belt where the respective roles of Atlantic and Pacific oceans are reversed, a greatly diminished Atlantic circulation with less significant changes in the Pacific circulation, and symmetric circulations in both the Pacific and Atlantic. The nature and magnitude of a perturbation required to turn the system into a different state have been hypothesized to occur from perturbations to either the surface freshwater budget or surface temperature (e.g. greenhouse warming). Modeled thermohaline circulations have collapsed on time scales of about 20 years. Positive feedback mechanisms can trigger instabilities of the circulation resulting in oscillatory phenomena. Observations and models suggest internal oscillations on time scales ranging from decades to millennia. The possibility that the ocean may switch from one state to another within a few decades is intriguing and indicates the importance of the interaction between the thermohaline circulation with the hydrological cycle.

Notes

An accessible treatment of feedback and control theory is given in *Feedback and Control Systems* (1967) by DiStefano et al.

Overviews of climate sensitivity and feedback analysis are given by Schlesinger (1986) and Hansen (1984).

An overview of the cloud-radiation feedback is given by Arking (1991).

An overview of feedbacks involving the ocean thermohaline circulation is given by Willebrand (1993).